STARS

University of Central Florida
STARS

Electronic Theses and Dissertations, 2004-2019

2011

Vision Based Trajectory Tracking Of Space Debris In Close Proximity Via Integrated Estimation And Control

Ni Li
University of Central Florida

Part of the Engineering Commons

Find similar works at: https://stars.library.ucf.edu/etd

University of Central Florida Libraries http://library.ucf.edu

STARS Citation

University of Central Florida

STARS
Showcase of Text, Archives, Research & Scholarship

VISION BASED TRAJECTORY TRACKING OF SPACE DEBRIS
IN CLOSE PROXIMITY VIA INTEGRATED ESTIMATION AND
CONTROL

by

NI LI
B.S. Northwestern Polytechnical University, 2008

A thesis submitted in partial fulfillment of the requirements
for the degree of Master of Science
in the Department of Mechanical, Materials & Aerospace Engineering
in the College of Engineering & Computer Science
at the University of Central Florida
Orlando, Florida

Spring Term
2011

Major Professor: Yunjun Xu

ABSTRACT

Since the launch of the first rocket by the scientists during the World War II , mankind continues their exploration of space. Those space explorations bring the benefits to human, such as high technology products like GPS, cell phone, etc. and in-depth insight of outside of the earth. However, they produce millions of debris with a total estimated mass of more than 3,000,000 kg in the space around the earth, which has and will continue to threat the safety of manned or unmanned space exploration. According to the research, at least tens of spacecraft were considered been damaged or destroyed by the debris left in the space.   Thus, the increasingly cluttered environment in space is placing a premium on techniques capable of tracking and estimating the trajectory of space debris.

Among debris, the pieces smaller than 1cm are unable to damage spacecraft because of the crafts' shields, while the pieces larger than 10cm can be tracked by ground-based radars or a radar network.   However, unlike the debris within these size ranges, the debris larger than 1 cm and smaller than 10 cm are able to hurt the shield of space craft and are hard to be detected by the exiting technical equipments because of their small size and cross-section area. Accordingly it is always a challenge for spacecraft or satellite mission designers to consider explicitly the ones ranged from 1 cm to 10 cm *a priori*.

To tackle this challenge, a vision based debris' trajectory tracking method is presented in the thesis. Unlike radar tracking, vision based tracking doesn't require knowledge of a debris' cross-section, regardless of its size.   In this work, two cameras onboard of satellites in a formation are used to track the debris in

close proximity. Also to differentiate the target debris from other clutters (i.e. the debris that are not tracked intentionally), a data association technique is investigated. A two-stage nonlinear robust controller is developed to adjust the attitude of the satellites such that the target debris is always inside of the field of view of the cameras. Capabilities of the proposed integrated estimation and control methods are validated in the simulations.

ACKNOWLEDGEMENTS

First of all, I would like to give sincere appreciation to my advisor Dr. Yunjun Xu for his immense academic insight, patient attitude on answering my questions and continuous support of my M.S study and research. I could not finish the M.S research and thesis without his guidance.

Besides my advisor, I would like to thank the rest of my thesis committee: Dr. Ilie Marcel and Dr. Lin Kuo-Chi, for their insightful comments, correction, and help on my thesis

I also want to thank my lab-mate Gareth Basset, who gives me useful suggestions on my research and English written.

Besides, I would like to thank my family and my friends, for standing behind me and supporting me spiritually throughout my life.

TABLE OF CONTENTS

LIST OF FIGURES

LIST OF TABLES

CHAPTER ONE: INTRODUCTION

Background of Debris Orbit Estimation

Risk of Space Debris

As a result of more than fifty years space exploration activities, more than million pieces of debris have been left in the space. According to the documents supplied by the NASA Orbital Debris Program Office [1] and Reference [2], the total number of debris ranging from 0.1-1cm is around 150 million, the debris ranging from 1-10cm is 650,000, and the debris larger than 10cm is 22,000.

The space debris has already and will continue to threaten human activities in space exploration [3-12]. Though the shielding technology such as Whipple shield can protect spacecrafts from damage of some debris, however, shield can only be used in limited missions, for example International Space Station [2, 13]. Moreover, as the development of solar panels and their widespread application in the field of space exploration, though most parts of spacecrafts can be protected by the shield, their solar panels which need to be exposed to the sun directly thus have high possibility to collide with the debris. The collision between solar panel and debris will result in generation of high-density plasma and breakdown of satellite component [10].

During the 50 years since the first man-made object into space were taken by German scientists, tens of space exploration activities were affected or failed because of the collision to the debris, such as the loss of French Military Satellite "Cerise", and orbit change of "NOAA7" Satellite, etc. [2,14]. One of the most recent ones is the loss of American operational satellite

which results from the collision with Russian un-operational satellite.

Space Debris Detection and Tracking

The potential dangerous of the space debris raises the concern for scientists since 1980s [15-16], up to now, several countries have jointly to detect and track the debris in the space, such as USA, UK, France, and Germany, etc.

Four kinds of methods are mainly used in practice to track debris, including ground based optical telescope, ground based radar, space based radar, and space based laser communication demonstration equipment.

(1) Ground based radar system or a radar network, such as the US SPACECOM, is convenient to detect and track the debris pieces larger than 10cm [17-18].

(2) Ground based optical telescope is also used to detect the debris in the size range of larger than 10cm [18]. One of the most famous telescopes is the ESA Space Debris Telescope, which is used to detect debris objects as small as 15cm.

(3) Space based radar suck like synthetic aperture radar (SAR) and inverse synthetic aperture radar (ISAR) [20-22] are applied to track the debris pieces within 1-10cm.

(4) By comparison, the space based laser demonstration equipment is most recently technology which is supposed to be unconstrained of the range of the debris size. According to Arimoto [23], a Laser Communications Demonstration Equipment (LCDE) is planned to be attached to the International Space Station (ISS) to observe the potential hazard of the space debris around ISS.

Motivation for the Research

Among debris, it always remains a challenge for smaller spacecraft or satellite mission

designers to explicitly consider *a priori* the debris ranging from 1 cm to 10 cm. Since the pieces smaller than 1cm are unable to damage spacecraft easily due to the development of crafts' material, while the pieces larger than 10cm can be tracked by ground-based radars or optical telescope system conveniently.

The newly developed technologies-space based radar and laser communication demonstration equipment can detect the debris within 1cm to 10cm. SAR and ISAR are independent of the background light, while the laser system can focus on a very tiny spots which is able to detect relatively smaller debris. However, both of them have limitations. For example, a post processing is typically required to reconstruct 2D images in ISAR and SAR. Also, the software and hardware design used those radars need to be modified each time according to debris pieces' sizes and orbits, which is not a cost-effective approach. For the space based laser equipment, it needs the downlink and uplink with ground systems which requires high performance of communication system. Besides, as a newly developed technology, laser equipment is only used to detect the debris, whether and how to use it to track the debris is still under investigation.

Moreover, recent researches [24-32] have shown the trend of scientists' willingness to remove debris by way of either destroying debris directly (i.e. using high power ground based laser), de-orbiting the debris (i.e. using electrodynamic space tether system) or capturing the debris and returning them to the ground (i.e. using robot arm). No matter which way to be used to remove debris, it is preferable that future spacecraft and satellites have the capability of estimating and tracking debris in close proximity autonomously without consistent communication with group stations.

In this thesis, an integrated vision based estimation and control approach is proposed to estimate the orbital information of the target debris via cameras aboard the cooperative satellites in a formation. The goal of the work is to track the target debris by differentiate it from other clutters, adjust the attitude of the satellites any time if necessary such that the desired field of view can be achieved for the target debris, and finally get the estimation orbit of the debris accurately.

<div align="center">Research Advantages</div>

The research outlined in this thesis focuses on: (1) the estimation of debris orbit in real-time by two pinhole cameras aboard a formation of small satellites instead of one heavy stereo camera aboard one large satellite; (2) the attitude of satellites is adjusted in a integrated approach such that the projected pixel location of the debris on the focal plane can be driven to a desired location by a newly developed nonlinear robust control technique which considers bounded functional and parametric uncertainties.

Three technical challenges are specifically addressed and solved in this thesis, shown as follows:

First, successive 2D images obtained through the vision sensors (e.g. light weight and low cost pinhole cameras) on two satellite platforms are coordinated to obtain the 3D position information of the debris. In addition to the obvious cost-reduction benefit as compared with the approach of using a stereo camera on a single large satellite [33], the formation satellite platform can increase the mission flexibility and observational baseline, and provide better survivability and reliability [34-39].

Second, to maintain the target debris within the cameras' fields of view, the attitude of

<div align="center">4</div>

the satellites will be controlled via a two-stage global asymptotically stable nonlinear output tracking controller. The advantage of this control is: the chattering is mitigated, especially when there is no large random noise in the plant model [40-43], therefore the controller will not induce large chattering due to the switching function. It is worth noting that different approaches [44-51] have been proposed to mitigate the chattering phenomenon in SMC. The method applied here doesn't involve low-pass filters, thus the steady state error will not be sacrificed. Also compared with dynamic inversion approaches, the controller developed here is robust with respect to functional and parametric uncertainties.

Third, the circumstances that multiple debris pieces may appear in the picture frames with high possibility, a probability data association (PDA) technique [52-53] combined with the Kalman filter will be investigated to differentiate the target debris from the clutter which has superiorities of less computational cost without much compromise in accuracy.

<u>Thesis Outline</u>

The overall structure of the integrated sensing and control strategy is first illustrated by diagram and discussed in Chapter 2.

In Chapter 3 of the thesis, the problem definition and cooperative estimation method are discussed. And the procedure of converting the debris ECI position to the pixel position on the image, of which projection involves a series of coordinate transformations from the Earth Centric Inertial (ECI), through the local vertical local horizontal (LVLH) coordinate of the satellite, the body coordinate of the satellite, and the body coordinate of the camera, to the focal plane of the camera, are also presented.

Considering the possibilities of one or more debris which are not necessary to considered

may appeared in the field of the camera, Chapter 4 applied PDA to estimate the debris orbit. The definition and background of data association and the reason to choose PDA method are first discussed. Then, the PDA method is illustrated in detail.

In Chapter 5 of the thesis, a nonlinear robust controller is described to maintain the debris inside of the cameras' fields of view. The mathematical theory of nonlinear robust output tracking control is described first. Then the structure and the detailed steps and equations of robust attitude control are illustrated.

To demonstrate the effectiveness of cooperative estimation in clutter, Chapter 6 presents an example of two micro satellites with two onboard cameras tracking the debris surrounded by two clutters. The simulation results and necessary interpretation and analysis are also presented.

Chapter 7 is a summary of thesis work and Chapter 8 is the challenge and future work concerning debris tracking.

CHAPTER TWO: OVERALL STRUCTURE

The overall structure of the integrated approach in estimating debris' trajectory is illustrated in Fig. 1.

```
                        ┌─────────────────┐
                        │  Space Debris   │
                        └─────────────────┘
                    ┌───────────┴───────────┐
                    ▼                       ▼
        ┌───────────────┐           ┌───────────────┐
   ┌───►│  Satellite 1  │           │  Satellite 2  │◄───┐
   │    └───────────────┘           └───────────────┘    │
┌──────────┐     │                         │      ┌──────────┐
│ Attitude │     ▼                         ▼      │ Attitude │
│ Control  │ ┌───────┐                 ┌───────┐  │ Control  │
└──────────┘ │ Pixel │                 │ Pixel │  └──────────┘
   ▲         └───────┘                 └───────┘     ▲
   └─────────────┘│                         │────────┘
                  ▼                         ▼
              ┌───────┐                 ┌───────┐
              │  PDA  │                 │  PDA  │
              └───────┘                 └───────┘
                  │                         │
                  └────►┌───────────┐◄──────┘
                        │ KF Filter │
                        └───────────┘
                              │
                              ▼
              ┌──────────────────────────────┐
              │ Debris' Trajectory Estimation │
              └──────────────────────────────┘
```
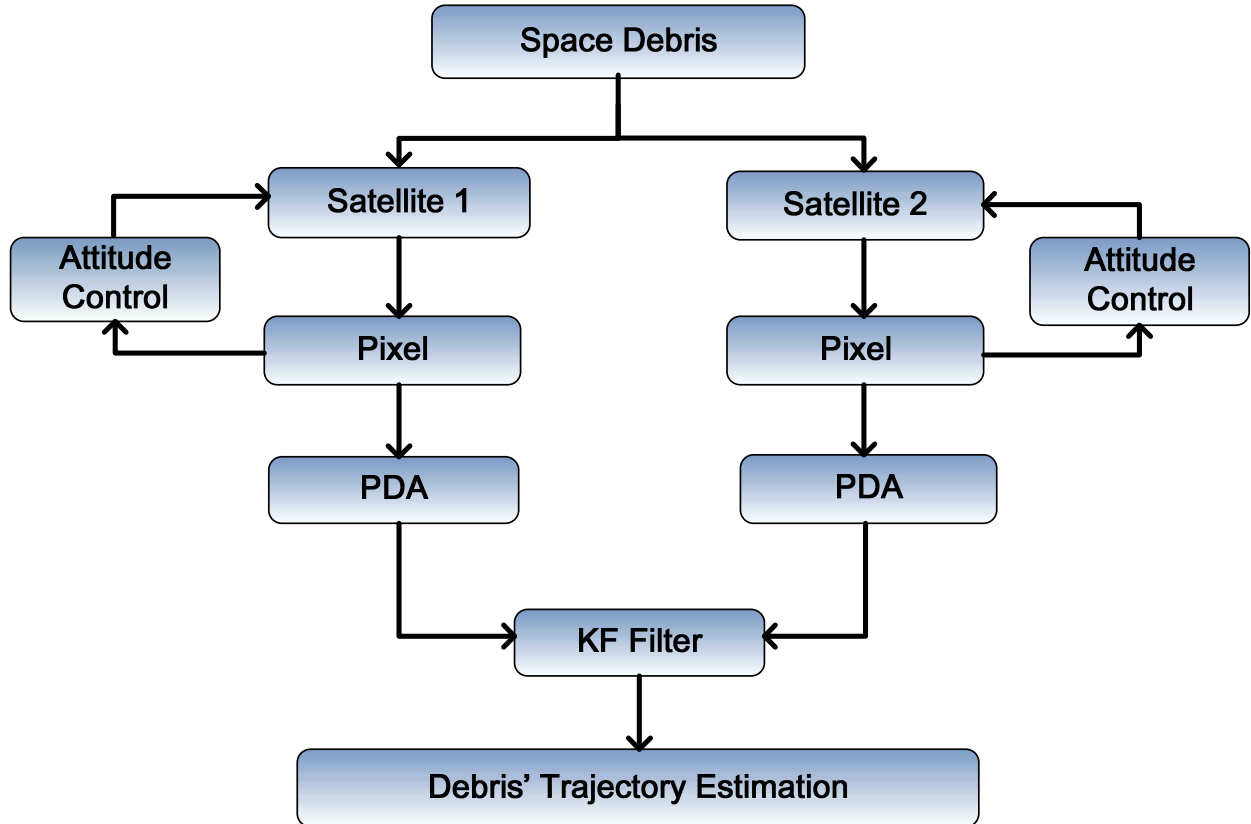
Figure 1: Overall Structure

To obtain the 3D position information of the debris, two cooperative satellites, each equipped with a pinhole camera, are used. The debris' projected pixel locations on the focal plane are used as the measurements of cameras. The PDA technique is designed in a decentralized approach to associate each of the possible measurements to the target of interest with a probability. After that, a Kalman filter based on the small disturbance model is designed to estimate the orbit of the debris in a centralized approach. In the meantime, the attitudes of

small satellites are controlled coherently such that the target debris is always inside of these two cameras' fields of view.

During the process of attitude control, the orbit estimation will temporarily stop updating, since the process of attitude control will lead to the unstableness of measurement of space debris shown on the image, which will further result in inaccuracy of the estimation. However, considering the large vision field of the camera and weak maneuverability of debris in the space, the estimation is still propagating without updating comparing with the measurements, and the propagation value will be used as desired position the cameras need to point to.

CHAPTER THREE: PROBLEM DEFINITION

Generation of State Model

The motion of the debris with an altitude larger than 200 km is governed by the following equation

$$\dot{r}_d = v_d$$
$$\dot{v}_d = -\left(\mu / r_d^3\right)r_d + w \tag{1}$$

in which the subscript d denotes the debris, $r_d \in \Re^{3\times1}$ and $v_d \in \Re^{3\times1}$ represent the position and velocity vectors of the debris in the Earth Centric Inertial (ECI) coordinate, respectively. r_d is the magnitude of the position vector. μ is the gravitational coefficient of the Earth. The drag, solar radiation pressure, and higher order gravitational terms, such as the J_2 perturbation are regarded as noise and represented by w. Here $w(t)$ is the vector of the zero-mean Gaussian process with an autocorrelation of $E[w(t)w(\tau)^T] = Q(t)\delta(t-\tau)$.

Here the small disturbance model derived based upon Eq. (1) is used as the processing dynamics in the PDA-KF design. Let's denote Eq. (1) as $\dot{x}_d = f(x_d) + w$, in which $x_d = [r_d, v_d]^T$. The nominal model is $\dot{x}_{d,0} = f(x_{d,0})$, in which the subscript "0" is used to denote the nominal values. The small disturbance model can be derived as $\Delta\dot{x}_d = A\Delta x_d + w$, where $A = (\partial f / \partial x_d)\big|_{x_{d,0}}$ and $\Delta x_d = x_d - x_{d,0}$.

Generation of Measurement Model

Coordinate Transformation

The measurement is the pixel location of the debris' position projected on the focal plane of the camera onboard of the small satellite.
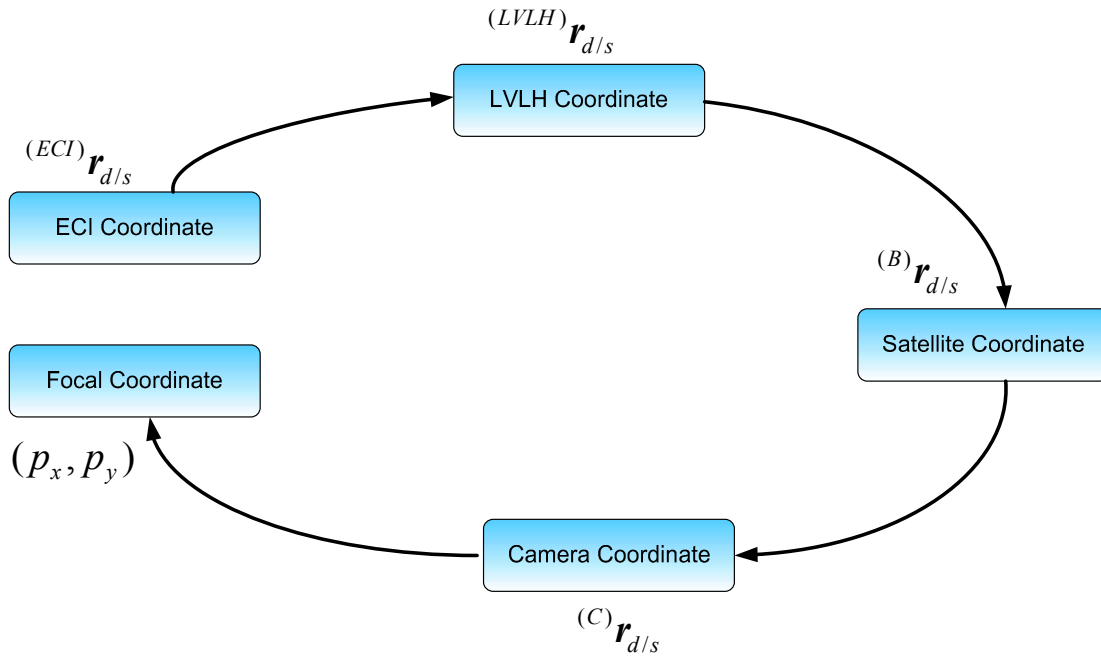
Figure 2: Coordinate Transformation

Shown as Fig. 2, the projection involves a series of coordinate transformations from the ECI, through the local vertical local horizontal (LVLH) coordinate of the satellite, the body coordinate of the satellite, and the body coordinate of the camera, to the focal plane of the camera. The detailed coordinate transformations are described next.

The position of the debris expressed in the LVLH can be written as

$$^{(LVLH)}\boldsymbol{r}_{d/s} = C_3(\nu + \omega)C_1(i)C_3(\Omega)\,^{(ECI)}\boldsymbol{r}_{d/s} \tag{2}$$

in which $\boldsymbol{r}_{d/s}$ $\boldsymbol{r}_d - \boldsymbol{r}_s$, and the subscript "s" represents the satellite. $^{(ECI)}\boldsymbol{r}_{d/s}$ is the relative

position between the debris and the satellite expressed in ECI. In this thesis, we use $C_\vartheta(\kappa)$ to denote the direct cosine matrix rotating about the axis ϑ (i.e. 1, 2, or 3) with an angle of κ. In Eq. (2), v, ω, i, and Ω are the true anomaly, argument of peripasis, inclination, and right ascension of the satellite orbit. The orbit elements of the small satellites are assumed to be constant in this thesis.

The relative position of the debris to the satellite $r_{d/s}$ expressed in the body coordinate of the satellite can be written as

$$^{(B)}r_{d/s} = C_1(\phi)C_2(\theta)C_3(\psi)^{(LVLH)}r_{d/s} \tag{3}$$

where the superscript B denotes the satellite body coordinate. The attitude of the small satellite is represented by the Euler angles $\sigma_s = [\phi, \theta, \psi]^T$, with a rotation sequence of 3-2-1.

The attitude motion of the small satellite is governed by

$$\begin{aligned}\dot{\sigma}_s &= R_1^{-1}\omega_s \\ \dot{\omega}_s &= -J_s^{-1}\tilde{\omega}_s J_s \omega_s + J_s^{-1}T\end{aligned} \tag{4}$$

where $\omega_s = [\omega_1, \omega_2, \omega_3]^T$ represents the angular velocity of the satellite. J_s is the moment of inertia of the satellite, and T is the control torque applied. It is worth noting that in both the estimation and control periods of the debris tracking mission, the rotation angle will be kept far away from 90o, therefore the singularity associated with the Euler representation case can be avoided. For the rotation sequence of 3-2-1, the rotation matrix R_1 can be derived as

$$R_1 = \begin{bmatrix} 1 & 0 & -\sin\theta \\ 0 & \cos\phi & \sin\phi\cos\theta \\ 0 & -\sin\phi & \cos\phi\cos\theta \end{bmatrix} \tag{5}$$

and the skew matrix of the angular velocity ω_s is defined as

$$\tilde{\boldsymbol{\omega}}_s = \begin{bmatrix} 0 & -\omega_3 & \omega_2 \\ \omega_3 & 0 & -\omega_1 \\ -\omega_2 & \omega_1 & 0 \end{bmatrix} \tag{6}$$

The relative position $\boldsymbol{r}_{d/s}$ expressed in the camera coordinate, denoted by the superscript "c", is

$$^{(C)}\boldsymbol{r}_{d/s} = [^{(C)}x_{d/s},\,^{(C)}y_{d/s},\,^{(C)}z_{d/s}]^T = \boldsymbol{R}_2{}^{(B)}\boldsymbol{r}_{d/s} + \boldsymbol{b}_{c/s} \tag{7}$$

As demonstrated in Fig. 3, $\boldsymbol{b}_{c/s}$ is the translational bias between the camera and satellite body coordinate, and $\boldsymbol{R}_2$ is the direct cosine matrix rotating from the satellite body coordinate to the camera coordinate. Without loss of generality, the camera is assumed to be installed along the negative y-axis of the satellite body coordinate, thus the rotation matrix $\boldsymbol{R}_2$ is

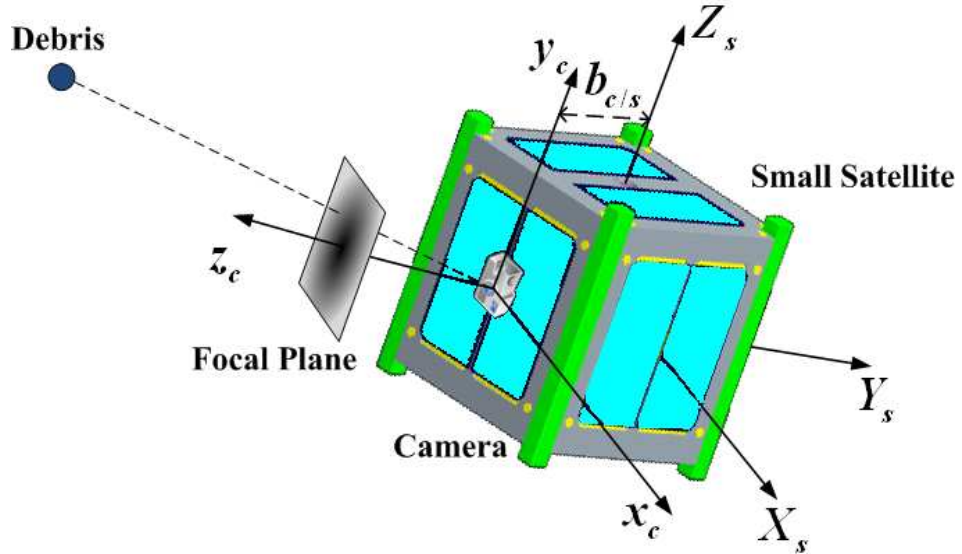$$\boldsymbol{R}_2 = \begin{bmatrix} 1 & 0 & 0 \\ 0 & 0 & 1 \\ 0 & -1 & 0 \end{bmatrix} \tag{8}$$

Figure 3: Camera Model

Finally, the pixel location of the debris, $[p_x, p_y]^T$, projected on the focal plane of the camera onboard, is calculated by,

$$p_x = k_1 f_c \frac{^{(C)}x_{d/c}}{^{(C)}z_{d/c}}$$
$$p_y = k_2 f_c \frac{^{(C)}y_{d/c}}{^{(C)}z_{d/c}}$$

(9)

where f_c is the focal length of the camera, k_1 is the ratio of the length of focal plane and length of pixel plane, and k_2 is the ratio of the width of focal plane and width of pixel plane.

Generation of Measurement

Through Eqs. (2)-(9), the measurement $[p_x, p_y]^T$ can be formulated as a function of x_d, x_s, and σ_s as $y = h(x_d, x_s, \sigma_s) + v(t)$, in which the noise $v(t)$ associated with the measurement is assumed to be a zero-mean Gaussian process with an autocorrelation of $E[v(t)v(\tau)^T] = R(t)\delta(t-\tau)$. Correspondingly, the nominal measurement model is $y_0 = h(x_{d,0}, x_s, \sigma_s)$, and the small disturbance model is derived as $\Delta y = H\Delta x_d + v$, where $H = (\partial h / \partial x_d)|_{x_{d,0}}$ and $\Delta y = y - y_0$ [54].

13

CHAPTER FOUR: COOPERATIVE ESTIMATION IN CLUTTER

Background of Data Association

The reason why data association is introduced in the thesis is that, if interfering targets exit and target are in the vision field of the camera simultaneously, the different measurements need to be associated with the same target so that we can get the accurate trajectory estimation. In another word, if more than one debris comes into the field view of the camera, correct measurements associated with the debris we are interested in need to be chosen or derived so that its orbit information can be got correctly.

Majority of the data association methods can be put into the following two categories: non-Bayesian approaches and Bayesian approaches.

(1) Non-Bayesian approaches include Nearest-neighbor filter (NNSF) and Track-splitting filter [52-55]. As the simplest approach, the NNSF method updates the state of the target using the measurement closest to the predicted value; however there is no guarantee that the nearest one will be the correct one. In the Track-splitting filter method, the track is split into separate hypotheses based on the number of the measurements within the validation region [52]. The likelihood function of each split track is computed and the most likely one is kept while all the others are discarded. However, this approach is not suitable for long time tracking and estimation problems due to its high computational and memory demands.

(2) Comparing with non-Bayesian approaches, Bayesian approaches [56-59], such as the PDA and the optimal Bayesian filter (OBA) methods, and improve the accuracy of estimation, since the "neighbors" of the predicted target are considered. The only difference between the

PDA and the OBA is that the OBA combines the association probabilities from initial up to the present time, while the PDA method only utilizes the association probabilities of the latest measurement. Because space debris is normally non-maneuverable, the association probabilities of the latest measurement are expected to be enough for updating the estimation of its trajectory. Therefore, the PDA method is chosen instead of the OBA method in this thesis, which will incur much less computational cost without much compromise in accuracy.

<div align="center">Probability Data Association Filter</div>

For brevity, only an outline of how to apply the PDA technique in this specific vision based debris estimation problem is given. The detailed information about the PDA method can be found in [52-53].

In each sampling time k, a validation set, defined by Eq. (10), is created, and only the measurements satisfying the constraint in Eq. (10) are considered as the validated measurements, while the other measurements will be discarded.

$$Z_k \quad \{ \boldsymbol{y}_{i,k} : \boldsymbol{d}_{i,k}^T(k) \boldsymbol{S}_k^{-1} \boldsymbol{d}_{i,k} \leq \gamma \}, \ i = 1, ..., m_k \tag{10}$$

Here, γ and m_k are the threshold of the validation set and the number of the measurements in the validation set at time step k, respectively. γ can be chosen according to the Chi Square distribution as described in [51], and the innovation $\boldsymbol{d}_{i,k}$ is calculated by

$$\boldsymbol{d}_{i,k} = \boldsymbol{y}_{i,k} - \hat{\boldsymbol{y}}_{k|k-1} \qquad , \ i = 1, ..., m_k \tag{11}$$

in which $\hat{\boldsymbol{y}}_{k|k-1}$ is the predicted measurement at step k based on the estimated value obtained at step $k-1$. The measurement prediction covariance $\boldsymbol{S}_k$ used in Eq. (10) will be discussed shortly. The cumulative set of measurements in the validated region up to the sampling time k

is defined to be $Z^k \quad \{Z_j, j = 1, ...k\}$.

Now, let's define the following two events: (1) Event $\theta_{i,k}$ is defined as the case when the validated measurement $\mathbf{y}_{i,k} \in Z_k$ is originated from the target debris. The conditional probability of this event $\beta_{i,k}$ is calculated by

$$\beta_{i,k} \quad P(\theta_{i,k} | Z^k) = e_{i,k} / (b + \sum_{j=1}^{m_k} e_{j,k}), \quad i = 1, ..., m_k \tag{12}$$

(2) Event $\theta_{0,k}$ is defined as the case when none of the validated measurement $\mathbf{y}_{i,k} \in Z_k$ is originated from the target debris, and the corresponding conditional probability $\beta_{0,k}$ is

$$\beta_{0,k} \quad P(\theta_{0,k} | Z^k) = b / (b + \sum_{j=1}^{m_k} e_{j,k}) \tag{13}$$

In Eqs. (12) and (13),

$$e_{j,k} = \exp\{-\frac{1}{2} d'_{j,k} S_k^{-1} d_{j,k}\} \tag{14}$$

$$b = (2\pi / \gamma)^{n_z/2} m_k C_{n_z} (1 - P_D P_G) / P_D \tag{15}$$

Here, n_z is the dimension of the measurement (i.e. two for the problem in this thesis) and C_{n_z} is the volume of the n_z dimensional unit hyper sphere (i.e. $C_{n_z} = \pi$ if $n_z = 2$). P_G is the probability that the measurement will fall in the threshold gate, and it will be fixed once γ and n_z are given. P_D is the probability that the true measurement is detected [53].

The measurement prediction covariance S_k used in Eq. (10), is propagated through

$$S_k = H_k P_{k|k-1} H_k^T + R \tag{16}$$

and

$$P_{k|k-1} = A_{k-1} P_{k-1|k-1} A_{k-1}^T + Q \tag{17}$$

respectively. The update equation of the error covariance is

$$P_{k|k} = \beta_{0,k} P_{k|k-1} + (1 - \beta_{0,k}) P_{k|k}^c + \tilde{P}_k \tag{18}$$

where

$$\tilde{P}_k = K_k \left[\sum_{i=1}^{m_k} \beta_{i,k} d_{i,k} d_{i,k}^T - d_k d_k^T \right] K_k^T \tag{19}$$

$$d_k = \sum_{i=1}^{m_k} \beta_{i,k} d_{i,k} \tag{20}$$

and the error covariance of the measurement that possibly originated from the target debris is

$$P_{k|k}^c = (1 - K_k H_k) P_{k|k-1} \tag{21}$$

In Eq. (21), K_k is the Kalman gain.

Then the updated states of the small disturbance model is given by

$$\Delta \hat{x}_{d,k|k} = \Delta \hat{x}_{d,k|k-1} + K_k d_k \tag{22}$$

At each step, once the small disturbance $\Delta \hat{x}_{d,k|k}$ is updated, the estimated position of the

debris can be calculated via

$$\hat{x}_{d,k} = x_{d,0,k} + \Delta \hat{x}_{d,k|k} \tag{23}$$

in which $x_{d,0,k}$ is the nominal value of the debris' trajectory at time step k [53].

CHAPTER FIVE: NONLINEAR ROBUST ATTITUDE CONTROL

Necessity of Nonlinear Robust Attitude Control

If the projected pixel location of the debris is very close to the boundary of the camera's field of view, the direction of camera, thus the attitude of the small/micro satellite, needs to be controlled such that the projected pixel location of the debris on the focal plane can be driven to a desired location, e.g. the center of the image.

The objectives of the attitude control are to (1) drive the pixel location of the debris to the desired position on the focal plane, and in the mean time, (2) regulate the angular velocity of the satellite to zero, and (3) maintain the Euler angle achieved when the projected pixel location of the debris reaches the desired position. It is worth noting that the system is an under-actuated system because there are only 3 control variables but 6 states need to be controlled.

Nonlinear Robust Output Tracking Control Theorems

In this work, we will employ a newly developed nonlinear robust control technique to solve this problem. Comparing with typical sliding mode control (SMC) approach, this chattering is mitigated, especially when there is no large random noise in the plant model. In the meantime, as comparing with typical dynamic inversion approaches, this controller is robust to bounded functional and parametric uncertainties. Here only the theorems are listed and the detailed asymptotically stability proof can be found in [47-49].

A nonlinear system with a state function is given by

$$x_i^{(n_i)} = f_i(\boldsymbol{x}_1,...,\boldsymbol{x}_n,t) + \sum_{j=1}^{m} b_{ij}(\boldsymbol{x}_1,...,\boldsymbol{x}_n)u_j, \; i=1,...,n, \; j=1,...,m \qquad (24)$$

and an output function of

$$y_i = h_i(x_1, \ldots, x_n), \ i = 1, \ldots, p \tag{25}$$

where $x_i = \left[x_i, \ldots, x_i^{(n_i-1)} \right]^T \in \mathfrak{R}^{n_i}$ and $x_i^{(n_i-1)} \quad d^{n_i-1} x_i / dt^{n_i-1}$ are the states with up to $n_i - 1$

derivatives. $\boldsymbol{u} = [u_1, \ldots, u_m]^T \in \mathfrak{R}^m$ is the control input and $\boldsymbol{B} = \left[b_{ij}(x_1, \ldots, x_n) \right] \in \mathfrak{R}^{n \times m}$ is the input

matrix with linearly independent vector fields. $\boldsymbol{f} = [f_1, \ldots, f_n]^T \in \mathfrak{R}^n$ is the nonlinear state

function.

The relative degree for $\boldsymbol{y} = \boldsymbol{h} = [y_1, \ldots, y_p]^T \in \mathfrak{R}^p$ is $\boldsymbol{r} = [r_1, \ldots, r_p]^T \in \mathfrak{R}^p$. It is worth noting

that $p \leq m$ is required because numerical errors of the controller need to be avoided. The aim of

the controller is to stabilize the system during the desired trajectory $y_{i,des}$, $i = 1, \ldots, p$ tracking,

where the subscript *des* denotes the desired signal. The nominal model is

$$\hat{x}_i^{(n_i)} = \hat{f}_i(x_1, \ldots, x_n, t) + \sum_{j=1}^{m} \hat{b}_{ij}(x_1, \ldots, x_n) u_j, \ i = 1, \ldots, n, \ j = 1, \ldots, m \tag{26}$$

and the nominal output is

$$\hat{y}_i = \hat{h}_i(x_1, \ldots, x_n), \ i = 1, \ldots, p \tag{27}$$

where $\wedge$ represents the nominal information, $\hat{\boldsymbol{f}} = [\hat{f}_1, \ldots, \hat{f}_n]^T \in \mathfrak{R}^n$ and

$\hat{\boldsymbol{B}} = \left[\hat{b}_{ij}(x_1, \ldots, x_n) \right] \in \mathfrak{R}^{n \times m}$.

$\left| \mathit{\Delta}_{ij} \right| \leq D_{ij} < 1$, $i, j = 1, \ldots, p$ is used to be the boundary of the parametric uncertainties of

the input matrix, as

$$(\boldsymbol{I} + \mathit{\Delta}) = \left[L_{\boldsymbol{B}} L_{\boldsymbol{f}}^{r-1} \boldsymbol{h}(\boldsymbol{x}) \right] \left[L_{\hat{\boldsymbol{B}}} L_{\hat{\boldsymbol{f}}}^{r-1} \hat{\boldsymbol{h}}(\boldsymbol{x}) \right]^+, \mathit{\Delta} \in \mathfrak{R}^{p \times p} \tag{28}$$

here, I is the identity matrix. "L" is the Lie derivative and "+" is the pseudo inverse.

The error between the nominal and actual state functions is bounded by

$F = [F_1, ..., F_p]^T \in \Re^p$ as

$$F_i = \left| -L_f^{r_i} h_i + L_{\hat{f}}^{r_i} \hat{h}_i \right|, \quad i = 1, ..., p \tag{29}$$

Let us define the sliding manifold $s = [s_1, ..., s_p]^T \in \Re^p$ as

$$s_i = \lambda_{-1,i} \int e_i dt + \sum_{k=0}^{r_i-2} \lambda_{k,i} e_i^{(k)} + e_i^{(r_i-1)}, \quad i = 1, ..., p \tag{30}$$

where $\lambda_{k,i} > 0$, $k = -1, ..., r_i - 2$, $i = 1, ... p$ can be any positive number. With a little bit abuse of

the symbol usage, the error signal is defined to be $e = [e_i] = \left[y_{i,d} - y_i \right]$, $i = 1, ..., p$.

The nonlinear robust control is shown in Theorem and Remark [48]:

Theorem: For a general nonlinear system (Eq. 24 and Eq. 25) with the bounded

parametric and functional uncertainties (Eq. 28 and Eq. 29), the proposed feedback control

scheme

$$u = \left[L_{\hat{B}} L_{\hat{f}}^{r-1} \hat{h}(x) \right]^+ \left[\frac{d^r y_{des}}{dt^r} - L_{\hat{f}}^r \hat{h}(x) + \lambda_{-1} \cdot e + \sum_{k=0}^{r-2} \lambda_k \cdot e^{(k+1)} + k \cdot s \right] \tag{31}$$

guarantees that the closed-loop system is globally asymptotically stable for tracking desired

signal $y_{i,des}$, $i = 1, ..., p$. Note that element-wise multiplication $a \cdot b = [a_1 b_1, ..., a_p b_p]^T \in \Re^p$ is

used. An explicit time varying feedback gain $k = [k_1, ..., k_p]^T \in \Re^p$ can be obtained from the

following equation

$$F + D \left| \frac{d^r y_{des}}{dt^r} - L_{\hat{f}}^r \hat{h}(x) + \lambda_{-1} \cdot e + \sum_{k=0}^{r-2} \lambda_k \cdot e^{(k+1)} \right| + \eta \cdot s = (I - D)k \cdot s \tag{32}$$

When $s_i = 0$, $k_i s_i$ instead of k_i will be calculated directly from Eq. (32) and used in Eq. (31).

Remark : It is worth noting that normally the uncertainty bound **F** and **D** cannot be obtained easily analytically. Therefore, in practice, try and error methods (e.g. through the Monte Carlo simulation) will be used to find these bounds as to be described in Chapter 6.

Structure of the Two-Stage Control

To achieve the control objectives mentioned above for the under-actuated system, a two-stage control strategy is proposed here.

As illustrated in Fig. 4, first the pixel location of the debris is driven to the desired position, e.g. the center of the image plane. At the same time, the angular velocity of the satellite is regulated to zero. After that, the Euler angles of satellite need to be maintained at the fixed value to ensure that the debris will stay within the field of view of camera for a relatively long duration.
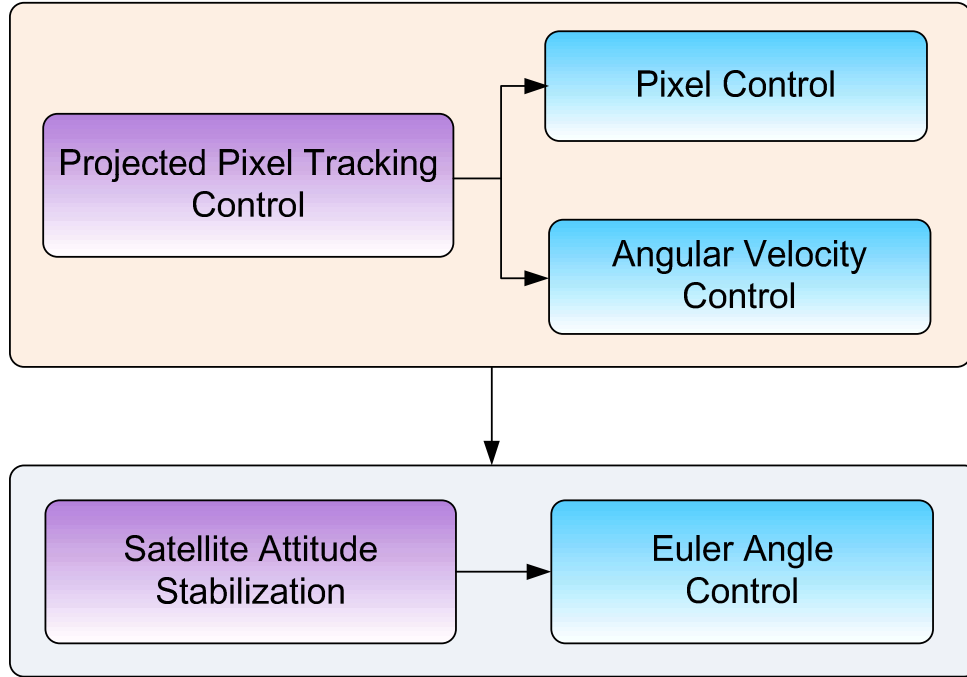
Figure 4: Overall structure of attitude control

<u>Stage 1: Projected Pixel Tracking Control</u>

In the first stage of the satellite attitude control, the pixel locations of the debris on both satellites' cameras need to be driven to the center of pixel plane, and in the meantime, the desired angular velocities of both satellites are zero.

Equation (4) is the state dynamics, in which the transpose of the input matrix $\boldsymbol{B}^T$ is $[\boldsymbol{0}, \boldsymbol{J}_s^{-1}]$. The state functions $\boldsymbol{f}$ includes two parts: $\boldsymbol{f}_1 = \boldsymbol{R}_1^{-1} \boldsymbol{\omega}_s$ and $\boldsymbol{f}_2 = -\boldsymbol{J}_s^{-1} \tilde{\boldsymbol{\omega}}_s \boldsymbol{J}_s \boldsymbol{\omega}_s$. The output of the controlled system is

$$y = \begin{bmatrix} y_1 \\ y_2 \end{bmatrix} = \begin{bmatrix} h_1 \\ h_2 \end{bmatrix} \tag{33}$$

in which h_1 is the pixel location of the debris position and h_2 is the angular velocity of the satellites.

22

The relative degree r of this system is $[2 \quad 2 \quad 1 \quad 1 \quad 1]^T$, and according to Theorem 1, the nonlinear robust controller has the following simplified form

$$u = \begin{bmatrix} L_{\hat{B}} L_{\hat{f}} \hat{h}_1 \\ L_{\hat{B}} \hat{h}_2 \end{bmatrix}^+ \left\{ \begin{bmatrix} \dfrac{d^2 y_{1,des}}{dt^2} \\ \dfrac{dy_{2,des}}{dt} \end{bmatrix} - \begin{bmatrix} L_{\hat{f}}^2 \hat{h}_1 \\ L_{\hat{f}} \hat{h}_2 \end{bmatrix} + \lambda_{-1} \cdot \begin{bmatrix} e_1 \\ e_2 \end{bmatrix} \\ + \begin{bmatrix} \lambda_0 \cdot e_1 \\ 0 \end{bmatrix} + k \cdot s \right\} \tag{34}$$

where

$$L_{\hat{B}} L_{\hat{f}} \hat{h}_1 = \frac{\partial}{\partial \hat{\omega}_s} \left(\frac{\partial \hat{h}_1}{\partial \hat{\sigma}_s} \hat{f}_1 \right) J_s^{-1} = \frac{\partial \hat{h}_1}{\partial \hat{\sigma}_s} \hat{R}_1^{-1} J_s^{-1} \tag{35}$$

$$L_{\hat{B}} \hat{h}_2 = J_s^{-1} \tag{36}$$

$$L_{\hat{f}}^2 \hat{h}_1 = \frac{\partial}{\partial \hat{\sigma}_s} \left(\frac{\partial \hat{h}_1}{\partial \hat{\sigma}_s} \hat{R}_1^{-1} \hat{\omega}_s \right) \hat{R}_1^{-1} \hat{\omega}_s - \frac{\partial \hat{h}_1}{\partial \hat{\sigma}_s} \hat{R}_1^{-1} J_s^{-1} \tilde{\hat{\omega}}_s J_s \hat{\omega}_s \tag{37}$$

$$L_{\hat{f}} \hat{h}_2 = \frac{\partial \hat{h}_2}{\partial \hat{\omega}_s} \hat{f}_2 \tag{38}$$

$$s = \begin{bmatrix} s_1 \\ s_2 \end{bmatrix} = \lambda_{-1} \cdot \begin{bmatrix} \int e_1 dt \\ \int e_2 dt \end{bmatrix} + \begin{bmatrix} \lambda_0 \cdot e_1 \\ 0 \end{bmatrix} + \begin{bmatrix} \dot{e}_1 \\ e_2 \end{bmatrix} \tag{39}$$

and

$$\begin{bmatrix} e_1 \\ e_2 \end{bmatrix} = \begin{bmatrix} y_{1,des} - \hat{y}_1 \\ y_{2,des} - \hat{y}_2 \end{bmatrix} \tag{40}$$

$y_{1,des}$ and $y_{2,des}$ are the desired pixel location and angular velocity, e.g. $[0 \quad 0]^T$ and $[0 \quad 0 \quad 0]^T$.

The control gain $k = [k_1, ..., k_5]^T$ are obtained from

$$(I - D)k \cdot s = F + D \left\| \begin{bmatrix} \dfrac{d^2 y_{1,des}}{dt^2} \\ \dfrac{dy_{2,des}}{dt} \end{bmatrix} - \begin{bmatrix} L_f^2 \hat{h}_1 \\ L_{\hat{f}} \hat{h}_2 \end{bmatrix} + \lambda_{-1} \cdot \begin{bmatrix} e_1 \\ e_2 \end{bmatrix} + \begin{bmatrix} \lambda_0 \cdot e_1 \\ 0 \end{bmatrix} \right\| + \eta \cdot s \quad (41)$$

and in the stage 1 controller

$$F = \left\| - \begin{bmatrix} L_f^2 h_1 \\ L_f h_2 \end{bmatrix} + \begin{bmatrix} L_f^2 \hat{h}_1 \\ L_f \hat{h}_2 \end{bmatrix} \right\| \quad (42)$$

is assumed to be the error bound between the predicted and actual state function. To guarantee

the asymptotically stability, λ_{-1}, λ_0 and η are required to be positive. The partial

derivative, $\dfrac{\partial}{\partial \hat{\boldsymbol{\sigma}}_s} \left(\dfrac{\partial \hat{h}_1}{\partial \hat{\boldsymbol{\sigma}}_s} \hat{R}_1^{-1} \hat{\boldsymbol{\omega}}_s \right)$, used in Eq. (37) is not straightforward, and the detailed

information is shown in Appendix.

<u>Stage 2: Small Satellite Attitude Stabilization</u>

To maintain the debris in the fields of view of the two cameras for a long time, the

attitude of satellite needs to be stabilized at the value achieved by the stage one controller.

Without fixing the Euler angle of satellites, the debris and the attitude of satellites may move to

different directions and result in pixels' quick drift to the boundary of the image plane. In this

stage, Eq. (4) is the state equation, while $y_3 = h_3 = \boldsymbol{\sigma}_s$ is controlled to the desired the Euler angle

of the satellite $y_{3,des} = \boldsymbol{\sigma}_{s,des}$. The relative degree $\boldsymbol{r}$ of the system is $[2 \quad 2 \quad 2]^T$, and the

nonlinear robust controller proposed in Theorem 1 can be simplified as

$$\boldsymbol{u} = \left[L_{\hat{B}} L_{\hat{f}} \hat{\boldsymbol{h}}_3 \right]^{-1} \left[\frac{d^2 y_{3,des}}{dt^2} - L_{\hat{f}}^2 \hat{\boldsymbol{h}}_3 + \lambda_{-1} \cdot e_3 + \lambda_0 \cdot \dot{e}_3 + k \cdot s_3 \right] \quad (43)$$

24

in which

$$L_{\hat{B}} L_{\hat{f}} \hat{h}_3 = \hat{R}_1^{-1} J_s^{-1} \tag{44}$$

$$L_{\hat{f}}^2 \hat{h}_3 = \left[\frac{\partial \hat{R}_1^{-1}}{\partial \hat{\omega}_s} \hat{\omega}_s \quad \hat{R}_1^{-1} \right] \begin{bmatrix} \hat{f}_1 \\ \hat{f}_2 \end{bmatrix} = \frac{\partial \hat{R}_1^{-1}}{\partial \sigma_s} \hat{\omega}_s \hat{f}_1 + \hat{R}_1^{-1} \hat{f}_2 \tag{45}$$

$$s_3 = \lambda_{-1} \cdot \int e_3 dt + \lambda_0 \cdot e_3 + \dot{e}_3 \tag{46}$$

and

$$e_3 = y_{3,des} - \hat{y}_3 \tag{47}$$

in which, $y_{3,des}$ is the Euler angles achieved at the end of control stage 1. The control gain

$k = [k_1, k_2, k_3]^T$ needs to satisfy

$$F + D \left| \frac{d^2 y_{3,des}}{dt^2} - L_{\hat{f}}^2 \hat{h}_3 + \lambda_{-1} \cdot e_3 + \lambda_0 \cdot \dot{e} \right| + \eta \cdot s_3 = (I - D) k \cdot s_3 \tag{48}$$

and in the stage 1 controller

$$F = \left| -L_f^2 h_3 + L_{\hat{f}}^2 \hat{h}_3 \right| \tag{49}$$

is assumed to be the error bound between the predicted and actual state function.

CHAPTER SIX: SIMULATION RESULTS

Simulation Scenario

The orbital information of the two micro satellites and the debris, used in the simulation, are listed in Table 1. It is assumed that initially both satellites have zero Euler angles and angular velocities. The moment of inertia of the satellite is obtained from the satellite platform developed at the University of Central Florida as

$$\boldsymbol{J}_s = \begin{bmatrix} 10662.54 & -40.20 & 73.65 \\ -40.20 & 10415.43 & 48.15 \\ 73.65 & 48.15 & 9618.74 \end{bmatrix} (\mathrm{g \cdot cm^2}) \qquad (50)$$

To demonstrate the effectiveness of the data associate technique applied in this thesis, two interference debris, i.e. two clutters, are generated around the target debris randomly.

Table 1 Orbital Information of the Satellites and Debris

Orbital information	Satellite 1/2, debris
Inclination	$30°/30°$, $20°$
Semi-major axis (km)	7500/7500, 7493
Eccentricity	0.1/0.1, 0.1
Right ascension	$10°/7°$, $35°$
Initial true anomaly	$8°/8°$, $8°$
Argument of periapsis	$90°/90°$, $70°$

The camera is located along the negative y axis of the satellite as shown in Fig. 2 with a focal length of $0.01m$, and the resolution of the images is chosen to be 480×360. The tuned parameters for the data association, estimation, and nonlinear robust controller are listed in Table

2. In the estimation part, the Gaussian noise associated with the processing dynamics is assumed to have a zero mean and covariance matrix of $\boldsymbol{Q} = 10^{-8}\boldsymbol{I}_3\ \mathrm{km}^2/s^4$ and Gaussian noise associated with measurement is assumed to have a zero mean and covariance matrix of $\boldsymbol{R} = \boldsymbol{I}_2$. The initial error covariance matrix is tuned to be $0.01\boldsymbol{I}_6$.

Table 2: Parameters Used in the Estimation and Control

Estimation	Value	Estimation	Value
P_G	0.9	γ	5
P_D	0.7	n_Z	4
Control		Stage 1/2	
λ_{-1}		$[5,5,1,1,1]^T / [10\ \ 10\ \ 10]^T$	
λ_0		$[3,3]^T / [1\ \ 1\ \ 1]^T$	
η		$[0.1,0.1,0.001,0.0005,0.001]^T /$ $[0.001\ \ 0.001\ \ 0.001]^T$	

The following uncertainties have been considered in the control section: the Euler angle is assumed to have 5% percentage errors, while errors in the angular velocity measurement are assumed to be 5%. Also the pixel location of the debris is the rounded to the nearest integer. As mentioned in Remark 2, the analytical bounds of $\boldsymbol{F}$ and $\boldsymbol{D}$ cannot be derived easily, and the Monte Carlo simulation is conducted in this thesis instead and $\boldsymbol{F}$ and $\boldsymbol{D}$ are found to be $0.1\left|L_{\hat{f}}^2\hat{\boldsymbol{h}}_3\right|$ and $0.4\boldsymbol{I}_3$ approximately.

<u>Simulation Results</u>

As shown in Figs. 5-7, the debris is initially inside of the two cameras' fields of view, thus the data associate and estimation methods are activated to estimate the debris' trajectory

among the clutters. After about 25 seconds, the pixel location of the debris of Satellite two is close to the boundary of the focal planes and thus the attitude control of both satellites are activated simultaneously. In the 50-second duration, the attitudes of these two satellites are controlled such that the pixel locations of the debris are driven to the center of image, i.e. $[0,0]$, and the angular velocities of the satellites are controlled simultaneously to zero with a stabilized Euler angle. After that, the estimation is resumed to track the target debris for about 350 seconds until the debris is out of camera's fields of view and attitude controllers are activated again. In Figs. 5-7, the section when the data association and estimation is activated is marked as "E", while the attitude control section is marked as "C".

As shown in Fig. 7, initially the target debris is close to the image boundary of the camera on the second satellite, therefore the estimation in the first "E" section is not fully settled down as shown in Figs. 5 and 6 after only 25 seconds. The capability of the proposed integrated approach is illustrated through the following attitude control section "C" and estimation section "E". The pixel locations of the target debris on two cameras are driven to the center, and the estimation error and the trace value of the error covariance matrix can reach their steady state in a relatively long duration before the debris drifts to the boundary of the image again.
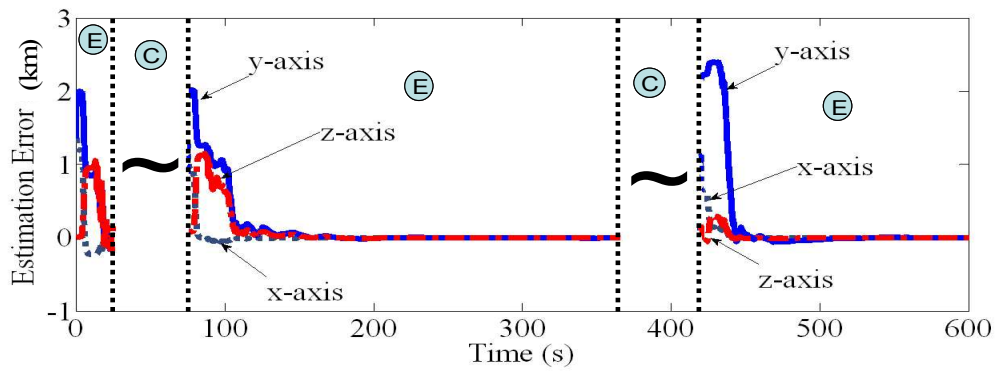
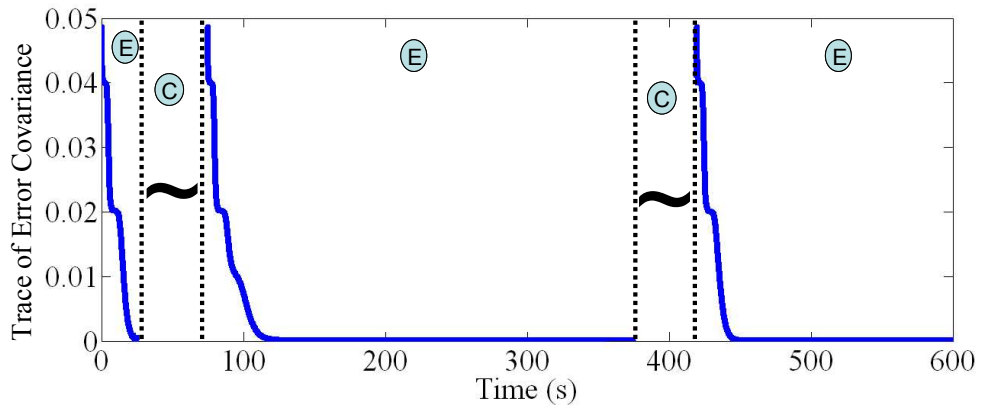Figure 5: Estimation Error of the Target Debris' Trajectory

Figure 6: Trace of the Error Covariance Matrix

Figure 7 shows the control performance of debris' projected pixels. Based on the assumption that only small disturbance existing in the nominal and real debris orbit, the attitude of satellite is controlled according to the projected pixel of nominal debris orbit.
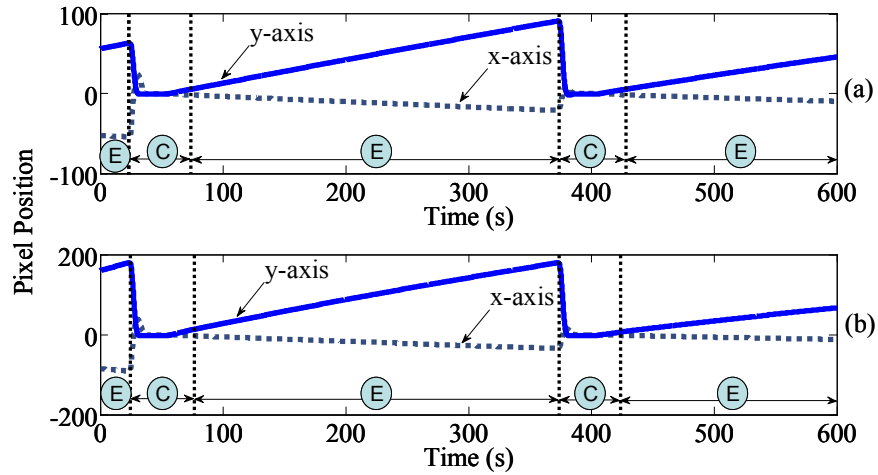
Figure 7: The Pixel Locations of the Debris on the Focal Plane of: a) Satellite One; b) Satellite Two

The detailed performance of the attitude control in Section "C" is illustrated in Fig.8 through Fig.15. As described in Section IV, the attitude control involves the projected pixel tracking control stage and the attitude stabilization stage, which are denoted by "C1" and "C2", respectively.

In Fig. 8 through Fig. 11, the Euler angles are controlled from their initial values, i.e. the Euler angles at the end of Section "E", to the desired ones so that the pixel of debris will be in the center of the focal planes. After 30 seconds, the stage-two controller is activated for both satellites, in which the angular velocities and the Euler angles of the satellites are maintained to be zero and the Euler angles achieved at the end of the control stage 1, respectively.

30
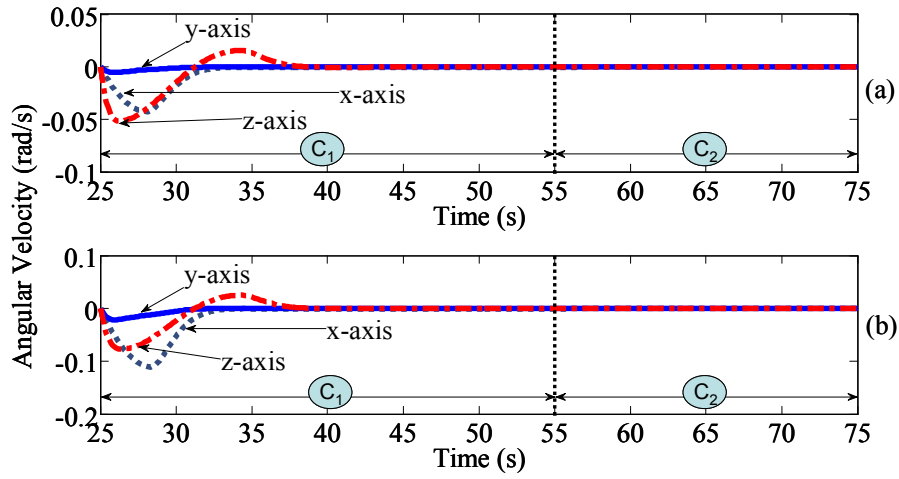
Figure 8: Angular Velocities of the Satellites in the 1st Attitude Control Period: a) Satellite One; b) Satellite Two
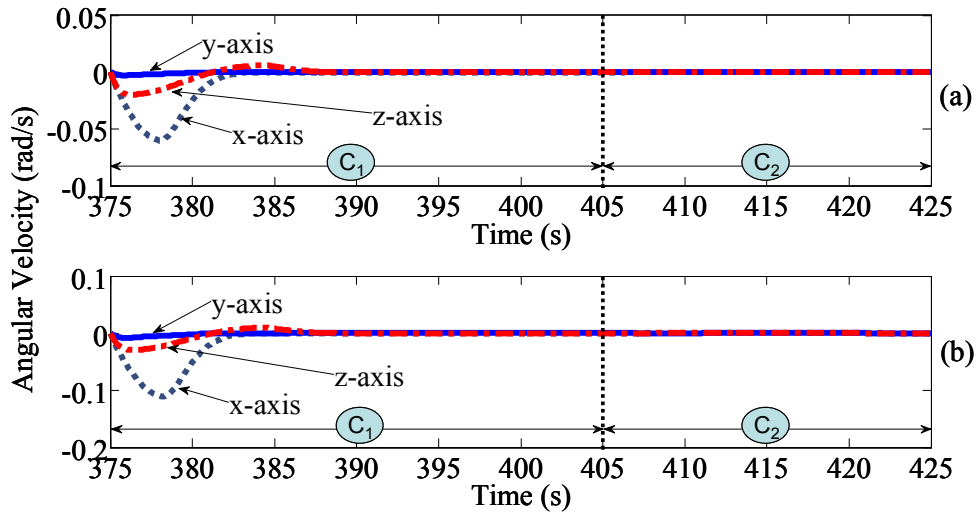
Figure 9: Angular Velocities of the Satellites in the 2nd Attitude Control Period: a) Satellite One; b) Satellite Two
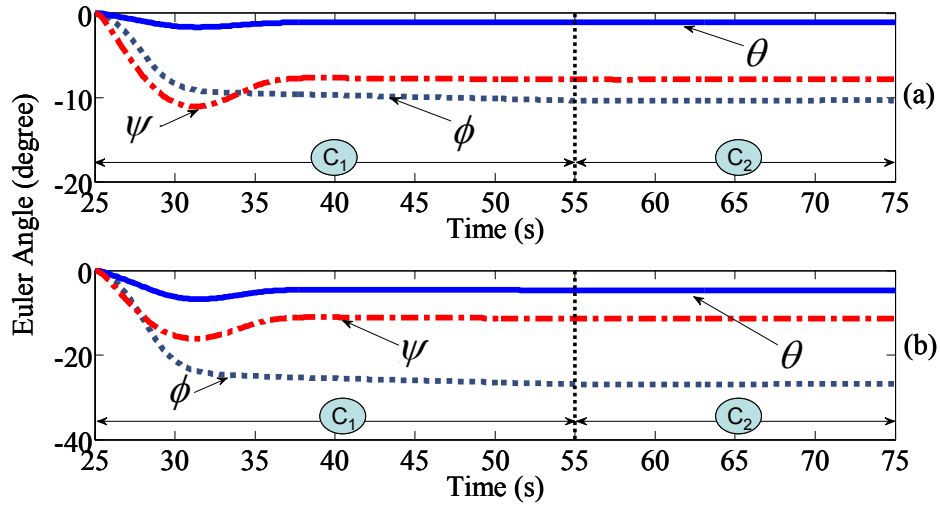
Figure 10: Euler Angles in the 1st Attitude Control Period: a) Satellite One; b) Satellite Two
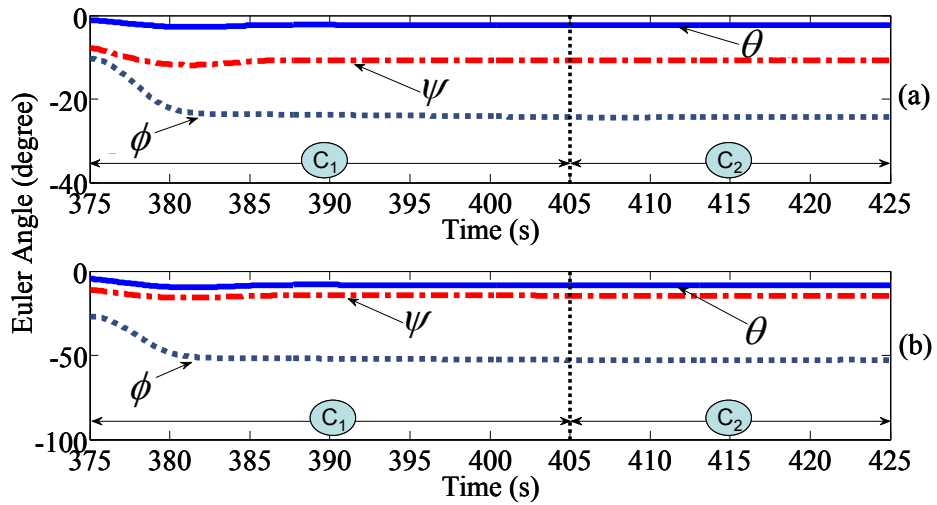
Figure 11: Euler Angles in the 2nd Attitude Control Period: a) Satellite One; b) Satellite Two

As demonstrated in Fig. 12 and Fig. 13, the torque commands generated by the proposed nonlinear robust control are chattering mitigation.
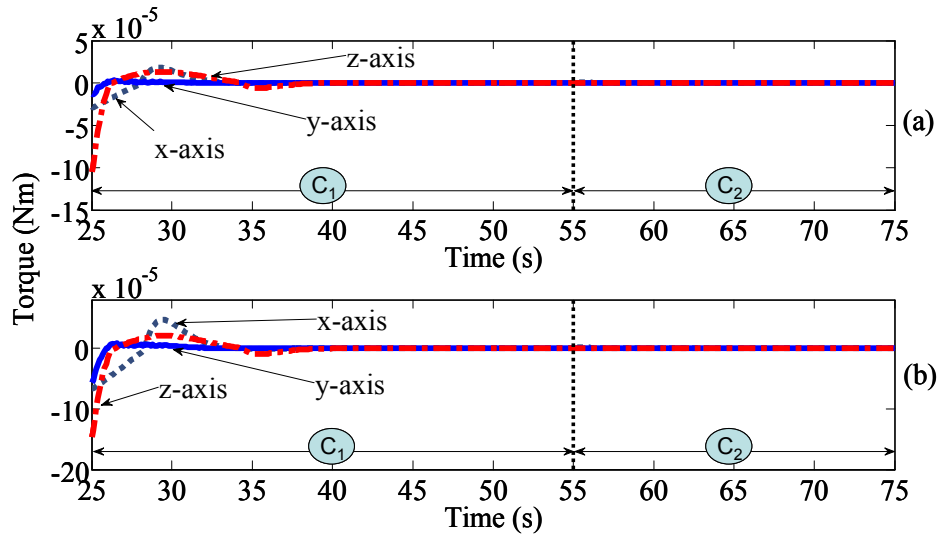
Figure 12: Torque Commands During the 1st Attitude Control Period: a) Satellite One; b) Satellite Two
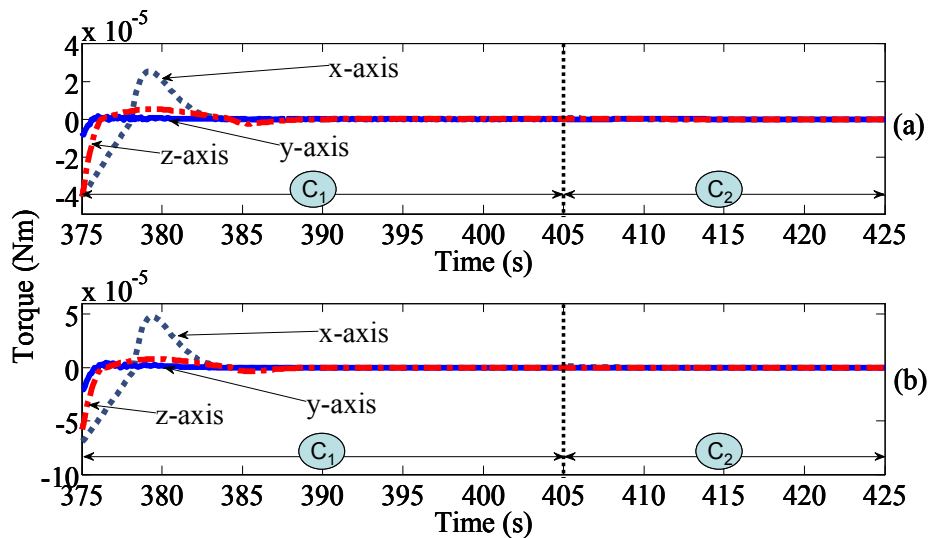
Figure 13: Torque Commands During the 2nd Attitude Control Period: a) Satellite One; b) Satellite Two

During the attitude control, the predicted pixel locations of the debris are shown in Figs. 14 and 15. It is worth noting that the pixel locations begin to drift in the stage-two control. The reason is that the debris is always moving, thus the projected pixels will be moving from desired location over time if only the attitude of the satellites is maintained in stage two.

33
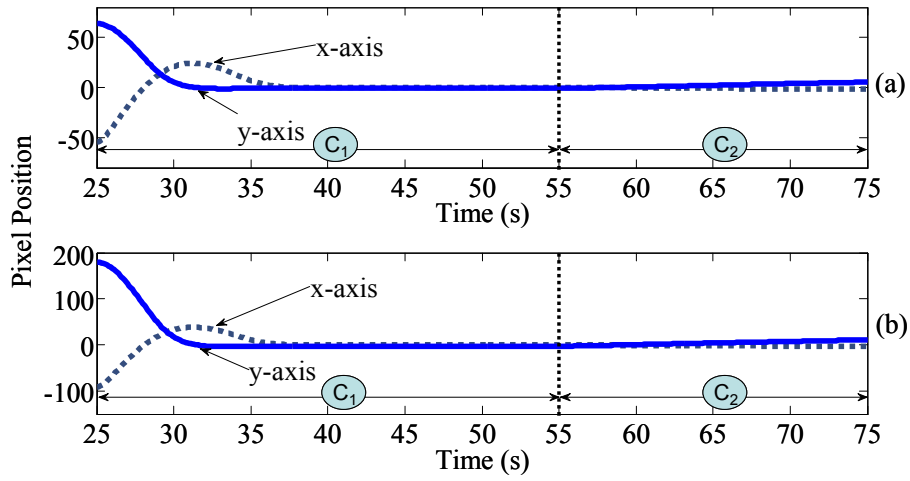
Figure 14: The Pixel Locations of the Debris in the 1st Attitude Control Period: a) Satellite One; b) Satellite Two
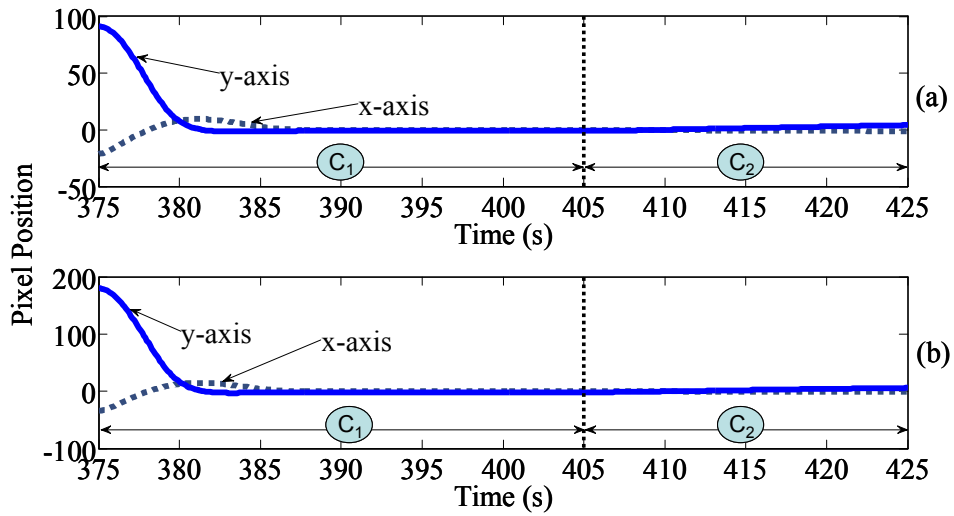
Figure 15: The Pixel Positions of the Debris in the 2nd Attitude Control Period: a) Satellite One; b) Satellite Two

CHAPTER SEVEN: SUMMARY AND CONCLUSION

In this work a vision based method, using 2D cameras aboard two satellites in a formation, is presented to track the debris in close proximity.

Three technical issues are addressed for the proposed approach: Successive 2D images obtained on two satellite platforms are coordinated to obtain the 3D position information of the debris. The attitude of the satellites is controlled via a two-stage asymptotically stable nonlinear output tracking controller so that the target debris can be maintained within the cameras' fields of view. The probability data association technique combined with the Kalman filter is developed to differentiate the target debris from the clutter. The simulation results demonstrate the effectiveness of the proposed methodology.

As compared with the other approaches such as using SAR, ISAR or a stereo camera on a single large satellite, the proposed method has the following advantages: cost reduction, avoidance of reconstruction of images, increased mission flexibility and observational baseline, and better survivability and reliability. Also, as the dramatically increase of the debris and complexity of the space exploration, it is necessary for future spacecraft and satellites have the capability of estimating and tracking debris in close proximity so that they are able to either avoid colliding with the debris or capture the debris autonomously without consistent communication with group stations.

CHAPTER EIGHT: FUTURE WORK

Currently the method can be applied only for estimating single debris target, so the extension of this work would be making the algorithm applicable for the problems involving multi debris targets and estimating the orbit information simultaneously to enhance the efficiency. A possible solution for this problem is introducing joint probabilistic data association (JPDA) in the estimation. Moreover, a challenge exists in the formation of two satellites, such as the alignment of satellites and the relative motion between satellites. In addition, because of the necessity to get rid of space debris, future research should take into account the size and shape of debris, which requires the detection technology and image processing knowledge.

APPENDIX: PARTIAL DERIVATIVES

The partial derivative $Z = \dfrac{\partial}{\partial \hat{\boldsymbol{\sigma}}_s}\left(\dfrac{\partial \hat{\boldsymbol{h}}_1}{\partial \hat{\boldsymbol{\sigma}}_s}\hat{\boldsymbol{R}}_1^{-1}\hat{\boldsymbol{\omega}}_s\right)$, used in Eq. (37), will be derived here step

by step.

The $(m,n)^{\text{th}}$ element of Z can be written as

$$Z_{m,n} = \frac{\partial}{\partial (\hat{\boldsymbol{\sigma}}_s)_n}\left(\frac{\partial \hat{\boldsymbol{h}}_1}{\partial \hat{\boldsymbol{\sigma}}_s}\hat{\boldsymbol{R}}_1^{-1}\hat{\boldsymbol{\omega}}_s\right)_m \qquad (51)$$

where

$$\left(\frac{\partial \hat{\boldsymbol{h}}_1}{\partial \hat{\boldsymbol{\sigma}}_s}\hat{\boldsymbol{R}}_1^{-1}\hat{\boldsymbol{\omega}}_s\right)_m = \sum_{k=1}^{3}\sum_{l=1}^{3}\frac{\partial (\hat{\boldsymbol{h}}_1)_m}{\partial (\hat{\boldsymbol{\sigma}}_{s,l})_l}(\boldsymbol{R}_1^{-1})_{l,k}(\hat{\boldsymbol{\omega}}_s)_k \qquad (52)$$

Thus

$$Z_{m,n} = \sum_{k=1}^{3}\sum_{l=1}^{3}\left[\frac{\partial^2 (\hat{\boldsymbol{h}}_1)_m}{\partial (\hat{\boldsymbol{\sigma}}_s)_l \partial (\hat{\boldsymbol{\sigma}}_s)_n}(\boldsymbol{R}_1^{-1})_{l,k}(\hat{\boldsymbol{\omega}}_s)_k + \frac{\partial (\hat{\boldsymbol{h}}_1)_m}{\partial (\hat{\boldsymbol{\sigma}}_s)_l}\frac{\partial (\boldsymbol{R}_1^{-1})_{l,k}}{\partial (\hat{\boldsymbol{\sigma}}_s)_n}(\hat{\boldsymbol{\omega}}_s)_k\right] \qquad (53)$$

To simplify the derivation, let's define $\hat{\boldsymbol{C}}_4 = \boldsymbol{C}_1(\hat{\phi})\boldsymbol{C}_2(\hat{\theta})\boldsymbol{C}_3(\hat{\psi})^{(LVLH)}$, $\boldsymbol{C}_5 = \boldsymbol{R}_2^{(B)}$, and

$\hat{\boldsymbol{V}} = \boldsymbol{C}_3(v+\omega)\boldsymbol{C}_1(i)\boldsymbol{C}_3(\Omega)^{(ECI)}\hat{\boldsymbol{r}}_{d/s}$, then $\hat{\boldsymbol{h}}_1 = [\hat{\boldsymbol{h}}_{11} \quad \hat{\boldsymbol{h}}_{12}]^T$ which represent the nominal pixel

position can be expressed as

$$(\hat{\boldsymbol{h}}_1)_m = d_m\frac{\displaystyle\sum_{l=1}^{3}\sum_{k=1}^{3}(\boldsymbol{C}_5)_{m,l}(\hat{\boldsymbol{C}}_4)_{l,k}(\hat{\boldsymbol{V}})_k + (\boldsymbol{b}_{c/s})_m}{\displaystyle\sum_{l=1}^{3}\sum_{k=1}^{3}(\boldsymbol{C}_5)_{3,l}(\hat{\boldsymbol{C}}_4)_{l,k}(\hat{\boldsymbol{V}})_k + (\boldsymbol{b}_{c/s})_3} = d_m\frac{L_2(\hat{\boldsymbol{\sigma}}_s)}{L_1(\hat{\boldsymbol{\sigma}}_s)}, m=1,2 \quad (54)$$

in which

$$[d_1 \quad d_2]^T = [k_1 f_c \quad k_2 f_c]^T \qquad (55)$$

where f_c is the focal length of the camera, k_1 is the ratio of the length of focal plane and length

of pixel plane, and k_2 is the ratio of the width of focal plane and width of pixel plane..

From Eqs. (54) and (55), the following equation can be derived.

$$\frac{\partial(\hat{\boldsymbol{h}}_1)_m}{\partial(\hat{\boldsymbol{\sigma}}_s)_l} = d_m \frac{1}{L_1^2(\hat{\boldsymbol{\sigma}}_s)}\left[L_1(\hat{\boldsymbol{\sigma}}_s)\frac{\partial L_2(\hat{\boldsymbol{\sigma}}_s)}{\partial(\hat{\boldsymbol{\sigma}}_s)_l} - L_2(\hat{\boldsymbol{\sigma}}_s)\frac{\partial L_1(\hat{\boldsymbol{\sigma}}_s)}{\partial(\hat{\boldsymbol{\sigma}}_s)_l}\right] \tag{56}$$

and

$$\frac{\partial(\hat{\boldsymbol{h}}_1)_m}{\partial(\hat{\boldsymbol{\sigma}}_s)_l\partial(\hat{\boldsymbol{\sigma}}_s)_n} = d_p \frac{1}{L_1^4(\hat{\boldsymbol{\sigma}}_s)}L_1^2(\hat{\boldsymbol{\sigma}}_s)$$

$$\left[\frac{\partial L_1(\hat{\boldsymbol{\sigma}}_s)}{\partial(\hat{\boldsymbol{\sigma}}_s)_n}\frac{\partial L_2(\hat{\boldsymbol{\sigma}}_s)}{\partial(\hat{\boldsymbol{\sigma}}_s)_l} + L_1(\hat{\boldsymbol{\sigma}}_s)\frac{\partial^2 L_2(\hat{\boldsymbol{\sigma}}_s)}{\partial(\hat{\boldsymbol{\sigma}}_s)_l\partial(\hat{\boldsymbol{\sigma}}_s)_n}\right.$$

$$\left.-\frac{\partial L_2(\hat{\boldsymbol{\sigma}}_s)}{\partial(\hat{\boldsymbol{\sigma}}_s)_n}\frac{\partial L_1(\hat{\boldsymbol{\sigma}}_s)}{\partial(\hat{\boldsymbol{\sigma}}_s)_l} - L_1(\hat{\boldsymbol{\sigma}}_s)\frac{\partial^2 L_1(\hat{\boldsymbol{\sigma}}_s)}{\partial(\hat{\boldsymbol{\sigma}}_s)_l\partial(\hat{\boldsymbol{\sigma}}_s)_n}\right]- \tag{57}$$

$$d_p\frac{1}{L_1^4(\hat{\boldsymbol{\sigma}}_s)}L_1^2(\hat{\boldsymbol{\sigma}}_s)\left[L_1(\hat{\boldsymbol{\sigma}}_s)\frac{\partial L_2(\hat{\boldsymbol{\sigma}}_s)}{\partial(\hat{\boldsymbol{\sigma}}_s)_l} - L_2(\boldsymbol{\sigma}_s)\frac{\partial L_1(\hat{\boldsymbol{\sigma}}_s)}{\partial(\hat{\boldsymbol{\sigma}}_s)_l}\right]2L_1(\hat{\boldsymbol{\sigma}}_s)\frac{\partial L_1(\hat{\boldsymbol{\sigma}}_s)}{\partial(\hat{\boldsymbol{\sigma}}_s)_n}$$

in which subscript $m \in [1,2]$ represents the values on the x axis and y axis respectively, i.e., $\hat{\boldsymbol{h}}_{11}$

and $\hat{\boldsymbol{h}}_{12}$ represent the nominal pixel position in x axis and y axis respectively, and

$$\frac{\partial L_1(\hat{\boldsymbol{\sigma}}_s)}{\partial(\hat{\boldsymbol{\sigma}}_s)_u} = \sum_{l=1}^{3}\sum_{k=1}^{3}(\boldsymbol{C}_5)_{3,l}\frac{\partial(\hat{\boldsymbol{C}}_4)_{l,k}}{\partial(\hat{\boldsymbol{\sigma}}_s)_u}(\hat{\boldsymbol{V}})_k \tag{58}$$

$$\frac{\partial L_2(\hat{\boldsymbol{\sigma}}_s)}{\partial(\hat{\boldsymbol{\sigma}}_s)_u} = \sum_{l=1}^{3}\sum_{k=1}^{3}(\boldsymbol{C}_5)_{m,l}\frac{\partial(\hat{\boldsymbol{C}}_4)_{l,k}}{\partial(\hat{\boldsymbol{\sigma}}_s)_u}(\hat{\boldsymbol{V}})_k \tag{59}$$

$$\frac{\partial^2 L_1(\hat{\boldsymbol{\sigma}}_s)}{\partial(\hat{\boldsymbol{\sigma}}_s)_u\partial(\hat{\boldsymbol{\sigma}}_s)_w} = \sum_{l=1}^{3}\sum_{k=1}^{3}(\boldsymbol{C}_5)_{3,l}\frac{\partial^2(\hat{\boldsymbol{C}}_4)_{l,k}}{\partial(\hat{\boldsymbol{\sigma}}_s)_u\partial(\hat{\boldsymbol{\sigma}}_s)_w}(\hat{\boldsymbol{V}})_k \tag{60}$$

$$\frac{\partial^2 L_2(\hat{\boldsymbol{\sigma}}_s)}{\partial(\hat{\boldsymbol{\sigma}}_s)_u\partial(\hat{\boldsymbol{\sigma}}_s)_w} = \sum_{l=1}^{3}\sum_{k=1}^{3}(\boldsymbol{C}_5)_{m,l}\frac{\partial^2(\hat{\boldsymbol{C}}_4)_{l,k}}{\partial(\hat{\boldsymbol{\sigma}}_s)_u\partial(\hat{\boldsymbol{\sigma}}_s)_w}(\hat{\boldsymbol{V}})_k \tag{61}$$

where, $(\Upsilon)_{a,b}$ represents $(a,b)^{\text{th}}$ element of the matrix Υ for example, $(\boldsymbol{C}_5)_{m,l}$ represents the

element in the mth row and l^{th} column of matrix $\boldsymbol{C}_5$, and $(\hat{V})_k$ represents the kth element of the

vector $\hat{V}$.

LIST OF REFERENCES

[1] NASA Orbital Debris Program Office website : http://orbitaldebris.jsc.nasa.gov/

[2] D. Wright, Space debris, Physics Today, S-0031-9228-0710-010-7

[3] J. J. Loughman, Overview and analysis of the SOLDIER satellite concept for removal of space debris, in: Proceedings of the AIAA SPACE 2010 Conference and Exposition, Anaheim, CA, 2010, Paper# AIAA 2010-8909.

[4] A. Molayath, Y. Khan, Studies on space debris tracking and elimination, in: Proceedings of the 46th AIAA/ASME/SAE/ASEE Joint Propulsion Conference and Exhibit, Nashville, TN, 2010, Paper# AIAA 2010-7008.

[5] E. Pate-Cornell, M. Sachon, Risks of particle hits during spacewalks in low earth orbit," IEEE Trans. Aerosp. Electron. Syst. 37 (1) (2001) 134-146.

[6] D. J. Heimerdinger, Orbital debris and associated space flight risks, in: Proceedings of 2005 Annual Reliability and Maintainability Symposium, Alexandria, VA, USA, 2005, pp. 508-513.

[7] C. Pardini, L. Anselmo, Assessing the risk of orbital debris impact," Space Debris, 1(1) (1999) 59-80.

[8] K. Gee, D. Mathias, Assessment of launch vehicle debris risk during ascent aborts, in: Proceedings of Reliability and Maintainability Symposium, Las Vegas, NV, US, 2008, pp.

70-73

[9] D. Mehrholz, L. Leushacke, W. Flury, R. Jehn, H. Klinkrad, M. Landgraf, Detecting, tracking and imaging space debris ESA Bulletin, 109 2002 128-134

[10] Y. Akahoshi, T. Nakamura, S. Fukushige, N. Furusawa, S. Kusunoki, Y. Machida, T. Koura, K. Watanabe, S. Hosoda, T. Fujita, M. Cho, Influence of space debris impact on solar array under power generation, International Journal of Impact Engineering 35 (2008) 1678-1682

[11] Guidelines and assessment procedures for limiting orbital debris, in: Proceedings of National Aeronautics and Space Administration, 1995, NSS 1740.14

[12] A. M. Bradley, L. M. Wein, Space debris: assessing risk and responsibility, Advances in Space Research, 43 (2009) 1372-1390

[13] http://www.esa.int/SPECIALS/ESOC/SEMZL0P256E_0.html

[14] T. Furniss, A history of space, Mercury Books, London, 2005

[15] I. Paz, J.R. Carl, R.W. Shaw, J.K. Kovitz, Design of an orbital debris radar ground demonstration, in: Proceedings of IEEE Aerospace Applications Conference, Breckenridge, CO, US, 1989, pp.1-15

[16] N.H. Fischer, R.C. Reynolds, Threat of space debris, in: Proceedings of IEEE Military Communications Conference, Los Angeles, CA, USA, 1984, pp. 397-406

[17] T. Sato, Shape estimation of space debris using single-range Doppler interferometry," IEEE

Trans. Geosci. Remote. Send. 37 (2) 1999 1000-1005.

[18] V.A. Chobotov, D.E. Herman, C.G. Johnson, Collision and debris hazard assessment for a Low-Earth-Orbit space constellation, J. Spacecr. Rocket. 34 (2) (1997) 233-238.

[19] J.G. Leu, A computer vision process to detect and track space debris using ground-based optical telephoto images. in: Proceedings of 11th IAPR Internation Conference on Pattern Recognition, Hague, 1992, pp. 522-525

[20] X.H. Cao, F.L. Su, H.D. Sun, G.D. Xu, Space debris observation via space-based ISAR imaging," in: Proceedings of the International Conference on Microwave and Milimeter Wave Technology, Builin, 2007, pp. 1-5.

[21] Q. Wang, M.D. Xing, Z. Bao, Space debris radar imaging, in: Proceedings of the 2007 IET International Conference on Radar Systems, Edinburgh, UK, 2007, pp. 1-3.

[22] J.R. Carl, G.D. Arndt, B.A. Bourgoise, I. Paz, Space-borne radar detection of orbital debris," in: Proceedings of 1993 Global Telecommunications Conference, Houston, TX, USA, 1993, pp. 939-943.

[23] Y. Arimoto, J. Uchida, A. Semerok, Space debris detection using Laser Communications Demonstration Equipment, in: Proceedings of IEEE Aerospace conference Proceedings Big Sky, MT, USA, 2000, pp. 85-91

[24] S.I. Nishida, T. Yoshikawa, A robotic small satellite for space debris capture, in: Proceedings of IEEE International Conference on Robotics and Biomimetics, Bangkok,

Thailand, 2009, pp. 1348-1353

[25] S.I. Nishida, T. Yoshikawa, Capture and motion braking of space debris by a space robot, in: Proceedings of International Conference on Control, Automation and Systems, Seoul, Korea, 2007, pp. 706-771

[26] S. Nakasuka, T. Fujiwara, New method of capturing tumbling object in space and its control aspects, in: Proceedings of IEEE International Conference on Control Applications, Kohala Coast, Hawi, USA, 1999, pp. 973-978

[27] S.I. Nishida, T. Yoshikawa, Space debris capture by a joint compliance controlled robot, in: Proceedings of IEEE International Conference on Advanced Intelligent Mechatronics, 2003, pp. 496-502

[28] D.K. Monroe, Space debris removal using high-power ground-based laser, Laser Power Beaming, 2121 (1994) pp. 276-283

[29] Y. Ishige, S. Kawamoto, S. Kibe, Study on electrodynamic tether system for space debris removal, Acta Astronautica, 55 (11) (2004) pp. 917-929

[30] R. P. Hoyt, P. Smith, The Remora Remover: a zero-debris method for on-demand disposal of unwanted LEO spacecraft, in: Proceedings of IEEE Aerospace Conferences, 2000, pp. 239-246

[31] D.N. Dimitrov, K. Yoshida, Utilization of the bias momentum approach for capturing a tumbling satellite, in: Proceedings of IEEE International Conference on Intelligent Robots

and Systems, Sendai, Japan, 2004, pp. 3333-3338

[32] V. Chobotov, N. Melamed, W. H. Ailor, W.S. Campbell, Ground assisted rendezvous with geosynchronous satellites for the disposal of space debris by means of Earth-oriented tethers. Acta Astronautica, 64 (9-10) (2009) pp. 946-951

[33] F. Terui, H. Kamimura, S. Nishida, Motion estimation to a failed satellite on orbit using stereo vision and 3D model matching, in: Proceedings of the 9th International Conference on Control, Automation, Robotics and Vision, Singapore, 2006, pp. 1-8.

[34] D.P. Scharf, F.Y. Hadaegh, S.R. Ploen, A survey of spacecraft formation flying guidance and control (part I): guidance, in: Proceedings of the American Control Conference, June 4-6, 2003, Denver, CO, pp. 1733-1739.

[35] C. Sultan, S. Seereram, R.K. Mehra, Deep space formation flying spacecraft path planning, Int. J. Robot. Res. 26 (4) (2007) 405-430.

[36] W. Ren, R.W. Beard, Formation feedback control for multiple spacecraft via virtual structures, IEEE Proc. Control. Theory Appl. 151 (3) (2004) 357-367.

[37] Y. Xu, Sliding mode control and optimization for 6 DOF satellites' formation flying considering saturation, J. Astronaut. Sci. 53 (4) (2005) 433-443.

[38] Y. Kim, M. Mesbahi, F.Y. Hadaegh, Dual-spacecraft formation flying in deep space: optimal collision-free reconfiguration, J. Guid. Control. Dyn. 26 (2) (2003) 375-379.

[39] J. Ward, S. Jason, M. Sweeting, Microsatellite constellation for disaster monitoring, in: 13th

AIAA/USU Conference on Small Satellites, SSC-99-V-2, August 23-26, 1999, Logan, UT.

[40] V. I. Utkin, Variable structure systems with sliding modes, IEEE Trans. Autom. Control. 22 (2) (1977) 212-222.

[41] G. Bartolini, E. Punta, T. Zolezzi, Simplex methods for nonlinear uncertain sliding-mode control, IEEE Trans. Autom. Control. 49 (6) (2004) 922-933.

[42] J.G. Lee, C.G. Park, H.W. Park, Sliding-mode controller design for spacecraft attitude tracking maneuvers," IEEE Trans. Aerosp. Electron. Syst. 29 (4) (1993) 1328-1333.

[43] J.E. Slotine, W. Li, Applied Nonlinear Control, New Jersey: Prentice Hall, 1990, pp. 267-307.

[44] G. Bartolini, A. Ferrara, E. Usai, V.I. Utkin, On multi-input chattering-free second order sliding mode control, IEEE Trans. Autom. Control. 45 (9) (2000) 1711-1717.

[45] J. Phuah, J. Lu, T. Yahagi, Chattering free sliding mode control in magnetic levitation system, Trans. Inst. Electr. Eng. Jpn. 125 (4) (2005) 600-606.

[46] B. Yao, M. Tomizuka, Smooth robust adaptive sliding mode control of manipulators with guaranteed transient performance, in: 1994 American Control Conference, Baltimore, MD, 1994, pp. 1176-1180.

[47] C.M. Lin, C.F. Hsu, Guidance law design by adaptive fuzzy sliding-mode control, J. Guid. Control. Dyn. 25 (2) (2002) 248-256.

[48] Y. Xu, Chattering free robust control for nonlinear systems, IEEE Trans. Control. Syst. Techno. 16 (6) (2008) 1352-1359.

[49] Y. Xu, Multi-timescale nonlinear robust control for a miniature helicopter, IEEE Trans. Aerosp. Electron. Syst. 46 (2) (2010) 656-671.

[50] D.R. Krupp, I.A. Shkolnikov, Y.B. Shtessel, High order sliding modes in dynamic sliding manifolds, SMC design with uncertain actuator, in: 2000 American Control Conference, June 2000, Chicago, IL, pp. 1124-1128.

[51] A. Levant, High-order sliding modes, differentiation and output-feedback control, Int. J. Control. 76 (9/10) (2003) 924-941.

[52] Y. Bar-Shalom, F. Daum, J. Huang, The probabilistic data association filter, IEEE Control. Syst. Mag. 29 (6) (2009) 82-100.

[53] Y. Bar-Shalom, T.E. Fortmann, Tracking and data association, Academic Press, Orlando, FL, 1988.

[54] D. Simon, Optimal state estimation, John Wiley & Sons, Hoboken, NJ, 2006.

[55] D. Musicki, B.F. La Scala, R.J. Evans, Integrated track splitting filter—efficient multi-scan single target tracking in clutter," IEEE Trans. Aerosp. Electron. Syst. 43 (4) (2007) 1409-1425.

[56] Y.S Kim, S.L. Choi, K.S. Hong, A suboptimal algorithm for the optimal Bayesian filter using receding horizon FIR filter," in: Proceedings of IEEE International Symposium on

Industrial Electronics, Pusan, South Korea, 2001, Vol. 3, pp. 1860-1865.

[57] J. Vermaak, S.J. Godsill, P. Perez, Monte Carlo filtering for multi-target tracking and data association," IEEE Trans. Aerosp. Electron. Syst. 41 (1) (2005) 309-332.

[58] K. Panta, B. Vo, S. Singh, Novel data association schemes for the probability hypothesis density filter," IEEE Trans. Aerosp. Electron. Syst. 43 (2) (2007) 556-570.

[59] M. Efe, D. Bonvi, Data association in clutter with an adaptive filter, in: Proceedings of the Fifth International Conference on Information Fusion, Annapolis, MD, Vol. 2, 2002, pp. 1243-1248.